Atmos. Chem. Phys. Discuss., 11, 17289–17336, 2011
www.atmos-chem-phys-discuss.net/11/17289/2011/
doi:10.5194/acpd-11-17289-2011

Atmospheric Chemistry and Physics Discussions

Aerosol concentration and size distribution measured below, in, and above cloud from the DOE G-1 during VOCALS-REx

L. I. Kleinman[1], P. H. Daum[1], Y.-N. Lee[1], E. R. Lewis[1], A. J. Sedlacek III[1], G. I. Senum[1], S. R. Springston[1], J. Wang[1], J. Hubbe[2], J. Jayne[3], Q. Min[4], S. S. Yum[5], and G. Allen[6]

[1]Brookhaven National Laboratory, Upton, New York, USA
[2]Pacific Northwest National Laboratory, Richland, Washington, USA
[3]Aerodyne Research Inc., Billerica, Massachusetts, USA
[4]State University of New York, Albany, New York, USA
[5]Yonsei University, Seoul, 120749, South Korea
[6]University of Manchester, Manchester, M13 9PL, UK

Received: 19 May 2011 – Accepted: 23 May 2011 – Published: 21 June 2011

Correspondence to: L. I. Kleinman (kleinman@bnl.gov)

Published by Copernicus Publications on behalf of the European Geosciences Union.

Abstract

During the VOCALS Regional Experiment, the DOE G-1 aircraft was used to sample a varying aerosol environment pertinent to properties of stratocumulus clouds over a longitude band extending 800 km west from the Chilean coast at Arica. Trace gas and aerosol measurements are presented as a function of longitude, altitude, and dew point in this study. Spatial distributions are consistent with an upper atmospheric source for O_3 and South American coastal sources for marine boundary layer (MBL) CO and aerosol, most of which is acidic sulfate in agreement with the dominant pollution source being SO_2 from Cu smelters and power plants. Pollutant layers in the free troposphere (FT) can be a result of emissions to the north in Peru or long range transport from the west. At a given altitude in the FT (up to 3 km), dew point varies by 40 °C with dry air descending from the upper atmospheric and moist air having a BL contribution. Ascent of BL air to a cold high altitude results in the condensation and precipitation removal of all but a few percent of BL water along with aerosol that served as CCN. Thus, aerosol volume decreases with dew point in the FT. Aerosol size spectra have a bimodal structure in the MBL and an intermediate diameter unimodal distribution in the FT. Comparing cloud droplet number concentration (CDNC) and pre-cloud aerosol ($D_p > 100$ nm) gives a linear relation up to a number concentration of $\sim 150\,cm^{-3}$, followed by a less than proportional increase in CDNC at higher aerosol number concentration. A number balance between below cloud aerosol and cloud droplets indicates that ~25 % of aerosol in the PCASP size range are interstitial (not activated). One hundred and two constant altitude cloud transects were identified and used to determine properties of interstitial aerosol. One transect is examined in detail as a case study. Approximately 25 to 50 % of aerosol with $D_p > 110$ nm were not activated, the difference between the two approaches possibly representing shattered cloud droplets or unknown artifact. CDNC and interstitial aerosol were anti-correlated in all cloud transects, consistent with the occurrence of dry in-cloud areas due to entrainment or circulation mixing.

ACPD
11, 17289–17336, 2011

1 Introduction

Satellite observations of cloud droplet effective radius indicate a gradient off the shore of Northern Chile. According to MODIS retrievals from the Aqua satellite for the month of October, average cloud droplet radius over the Pacific Ocean increased from 8 to 14 µm from the coast to 1000 km offshore (Wood et al., 2007). This gradient is plausibly attributed to anthropogenic aerosol sources from Cu smelters, power plants, and urban areas in Chile and Peru.

Anthropogenic perturbations to marine stratocumulus clouds was one motivation for the VAMOS Ocean-Cloud-Climate-Atmosphere-Land Regional Experiment (VOCALS-REx or VOCALS, for short), an overview of which is provided by Wood et al. (2011). The US DOE G-1 aircraft participated in the international collaboration described by Wood et al. Aboard the G-1 were instruments for in-situ measurements of cloud microphysics, aerosol concentration, size distribution, and composition, gasses useful as air mass tracers, and navigational and meteorological parameters. The sampling region of the G-1 extended from Arica, Chile, 800 km west to 78° W mainly within a restricted latitude band between Arica at 18.35° S and 20° S.

Allen et al. (2011) have summarized meteorological conditions and the chemical composition of the boundary layer and free troposphere within one degree of 20° S between the coast of Chile and 85° W, relying on aircraft measurements from the UK BAe 146, NSF C130, and DOE G-1, supplemented by surface observations from the research vessel Ronald H. Brown. Allen et al. (2011) provide multiple comparisons between platforms which, in general, reveals a high degree of consistency. Bretherton et al. (2010), relying principally on the C130, and BAe146 long range aircraft, provide a comprehensive synthesis of marine boundary layer and free troposphere structure, clouds, and precipitation along the 20° S corridor. Further information on the marine boundary layer and aerosol source attribution is given in Rahn and Garreaud (2010) and Chand et al. (2010), respectively. In this study we provide a more complete treatment of aerosol and trace gas measurements from the DOE G-1 with emphasis on

ACPD
11, 17289–17336, 2011

the longitudinal and vertical distribution of aerosol concentration and size distribution. Summary information is provided on aerosol composition derived from AMS and PILS measurements, the primary description of which will be contained in an article by Lee et al. (2011).

Data are presented for the entire field campaign, segregated into subsets according to longitude, altitude, dew point temperature (T_d), or whether measurements are below, in, or above cloud. We find that dew point is a better indicator of air mass type and origin then altitude and thus trends of trace gasses or aerosol as a function of dew point often show less scatter than the same trends considered as a function of altitude.

The concentration and size distribution of interstitial aerosol are described. These are particles observed in-cloud that either never grew into cloud droplets (i.e., were not activated) or having been activated are returned to the gas phase by cloud droplet evaporation. Properties of interstitial aerosol depend on many variables such as aerosol size and composition, cloud updraft velocity, and entrainment of dry air. A simplifying feature of the VOCALS observations is that bulk measurements of aerosol composition indicate a relatively uniform composition of easily activated particles. Constant altitude cloud transects were identified and for these transects an average aerosol size distribution was calculated as a function of liquid water content, which is compared with an average size distribution determined from the no-cloud water transect portions. The fraction of interstitial accumulation mode size aerosol was higher than could be explained from an adiabatic parcel model, suggesting the importance of entrainment. In each of 102 cloud transects there is a negative correlation of cloud droplet number concentration with accumulation mode aerosol. One transect has been selected as a case study and used to further illustrate aerosol and cloud droplet variability.

2 Experimental

Aerosol properties are reported at ambient temperature and pressure. Local daylight savings times equal to UTC-3 are used in this study. Data are archived at ftp://ftp.asd.bnl.gov/pub/ASP%20Field%20Programs/2008VOCALS/, which uses UTC time.

ACPD
11, 17289–17336, 2011

2.1 Instruments

Aerosol and cloud instruments used in this study are listed in Table 1. The G-1 had its usual navigational and meteorological package for measuring position, winds, temperature, and dew point http://www.pnl.gov/atmospheric/programs/raf.stm. CO and O_3 were used as air mass tracers. CO was determined by VUV resonance fluorescence (Resonance Ltd., Barrie, ON, Canada). Ozone was measured by a modified UV absorption detector (Model 49-100, Thermo Electron Corporation, Franklin, MA). SO_2 measurements from a modified pulsed fluorescence detector (Model 43S, Thermo Electron Corporation, Franklin, MA) were typically below a 200 ppt limit of detection. Further information on gas phase instruments used in VOCALS can be found in Springston et al. (2005) and Kleinman et al. (2007).

2.1.1 Aerosol composition

Aerosol composition was measured via an AMS and PILS and acidity determined by NH_4^+ to SO_4^{2-} ratio and conductivity as described by Lee et al. (2011). They found that nonrefractory, sub-micron size aerosol in the marine boundary layer had an average composition between $(NH_4)HSO_4$ and H_2SO_4 with a 10–15 % admixture of organics. Acidic aerosol with this composition contains significant water even at low relative humidity (RH) (Lee et al., 2011). Based on the E-AIM website, http://www.aim.env.uea.ac.uk/aim/aim.php, (Clegg et al., 1998) a solution consisting of 30 molal each NH_4HSO_4 and H_2SO_4 is calculated to be in equilibrium at the ~ 15 % RH used for particle size measurements. The density of this solution is 1.56 g cm^{-3} at 298.15 °K, insensitive to temperature (Clegg and Wexler, 2011). If an insoluble organic component with density 1.2 g cm^{-3} comprises 10 % of the aerosol mass, then the volume growth factor at 15 % RH (calculated as the sum of the volumes of the solution and organic component divided by the sums of the volumes of the solutes and the organic component), is equal to 1.29, and the radial growth factor is 1.09.

ACPD
11, 17289–17336, 2011

2.1.2 Aerosol size distributions

Size distributions of aerosol particles in the Aitken and accumulation mode were quantified with one minute time resolution using an SMPS (scanning mobility particle sizer) consisting of a cylindrical differential mobility analyzer (DMA) and a condensation particle counter. It is assumed that particles are spherical so that mobility and geometric diameters are equal. Data were analyzed using the inversion algorithms described by Collins et al. (2002). A Nafion dryer upwind of the DMA reduced RH to 14 % ($1\sigma = 2$ %). In reporting "dry" size distributions in this article, water of hydration at 15 % RH is not taken into account. Reported particle diameters are thus approximately 9 % larger than in the dry state. In the case where there are few particles below the 15 nm lower limit of detection of the SMPS, the total number of particles in the size range 15–440 nm should be a good approximation for CN. Comparisons between the CPC3010 ($D_p > 10$ nm) and the SMPS generally show agreement within 10 % for sampling periods without appreciable concentrations of small particles.

Two Passive Cavity Aerosol Spectrometer (PCASP) units were used to measure aerosol with nominal diameter between 0.1 and 3 µm. One PCASP was mounted on a pylon on the nose of the aircraft and the other located inside the cabin. In the data archive the two PCASPs are identified as units A and B. Midway through the program these units were switched, so that from the start of the program through 28 October, unit A was outside and unit B inside. From 29 October till the end of the VOCALS campaign, unit B was outside and unit A inside. The relative humidity of air sampled by both PCASPs was decreased by the use of deicing heaters which yield about a 20 °C increase in temperature (Haller et al., 2006). Cabin heat also contributed to the drying of aerosol measured inside the aircraft.

PCASP data reported in the data archive were generated using size bins based on spherical particles with a refractive index (RI) of 1.55. In this study, size bins were adjusted to an RI of H_2SO_4 (1.41) using Mie scattering results from Liu and Daum (2000). This is close to the volume weighted refractive index determined from non-volatile

ACPD
11, 17289–17336, 2011

components of sub micrometer size aerosol measured by the AMS (RI=1.46). Addition of retained water (RI=1.33) results in a lower refractive index, close to 1.41.

Comparisons were made between aerosol volume determined by the SMPS and the two PCASPs. In order to match size ranges, volumes are calculated for D_p between 0.11 and 0.44 µm. A linear regression of PCASP A volume vs. SMPS volume had a slope of 0.84 and $r^2 = 0.91$; for PCASP B the slope and r^2 were 0.98 and 0.93, respectively. Agreement is well within the 30 % uncertainty limits typically cited for PCASP and SMPS volume measurements. Volumes determined by PCASP A and B vary by only a few percent according to which unit is inside or outside of the aircraft.

PCASP and SMPS number distributions differed, primarily due to a low detection efficiency of small particles in the PCASP ($D_p < 160$ nm), which was confirmed only recently in a post-flight calibration of PCASP A. PCASP size distributions were adjusted to match those from the SMPS. A set of global adjustment factors to be applied to all PCASP data were determined by performing a linear regression between the SMPS and PCASP A and PCASP B for 15 size bins. All non-cloud data were used for these regressions. To test the normalization procedure, plots were made of PCASP vs. SMPS number concentration integrated over the overlap size range 110–440 nm (not shown). A least squares regression yields slopes of 0.95 and 0.96 for PCASP A and B vs. SMPS, respectively, both with an r^2 of 0.85. By construction slopes should be close to unity. Scatter in the number comparisons is a measure of how well a single set of adjustment factors works in the differing environments encountered over 16 flights. Normalization resulted in an increase of total particle concentration by 41 % and 18 % from PCASP A and PCASP B, respectively.

By adjusting the PCASP data, we are relying on the SMPS as providing an intrinsically more accurate size distribution. The adjustment procedure allows for the determination of number concentrations and size distributions with 1 s time resolution using PCASP data which on average agrees with the SMPS. Fast response aerosol number concentrations will prove useful in examining the anti-correlation between cloud droplets and interstitial aerosol.

ACPD
11, 17289–17336, 2011

2.1.3 Cloud microphysics

Cloud droplet number concentration (CDNC) was determined via a Cloud and Aerosol Spectrometer (CAS) probe manufactured by Droplet Measurement Technologies (DMT). Results were integrated over a diameter range between 2.5 and 50 µm. Cloud liquid water content (LWC) was measured with a Particle Volume Monitor (PVM, Gerber et al., 1994) and checked against a hot wire detector. Drizzle concentration was determined from a DMT Cloud Imaging Probe (CIP) which together with the CAS and hot wire detector are packaged together as a Cloud, Aerosol, and Precipitation Spectrometer (CAPS), mounted on a pylon off the nose of the G-1. Data has been archived at 0.1, 1, and 10 Hz, and is available on request at 40 and in some cases 200 Hz.

2.2 Flights

Figure 1 shows the 3-D sampling region of the G-1 during 16 of 17 research flights. An electrical failure on 18 October limited data collection and that flight is not used in this study. Instrument status and flight times are tabulated in spreadsheet format on the same ftp site as the data. Flight duration was approximately 4 h. Thirteen of 16 flights started between 08:57 and 10:20 (11:57 and 13:20 UTC).

Flight objectives were to determine the horizontal and vertical variability of cloud and aerosol properties. The range of the G-1 allowed for sampling between Arica at 70.3° W out over the Pacific to 78° W, an E–W distance of 800 km. Vertical sampling was done either via multiple transects at different altitudes, ascents and descents through clouds typically at vertical velocities of 1000 ft min^{-1}, or by porposing between cloud and above-cloud regions.

A typical flight track designed to sample longitudinal variations in cloud and aerosol properties is shown in Fig. 2. Because clouds thinned and sometimes disappeared due to solar heating as the day progressed, the out bound leg was usually devoted to cloud sampling and the inbound leg to sampling in the boundary layer below cloud height. In order to examine interstitial aerosol, 102 constant altitude transects were identified

ACPD
11, 17289–17336, 2011

in which the maximum liquid water content (LWC) was at least 0.1 g m^{-3}. Often there were multiple transects in a single cloud separated by a step change in altitude of order tens of m or greater. For many transects clouds were broken or occupied only a portion of the transect. The non-cloud (LWC < 0.01 g m^{-3}) portion of these transects defines precloud aerosol that can be compared with interstitial size distributions as a function of LWC. One cloud on Flight 081028a (Fig. 2) is singled out as a case study to illustrate the anti-correlation between cloud droplet number concentration and interstitial aerosol found in all 102 cloud transects. As described in Sect. 3.3, an alternate definition of pre-cloud aerosol related to aerosol below cloud height is used to quantify the first indirect effect.

As indicated in Fig. 3, aerosol number concentration measured by SMPS was nearly the same on outbound and inbound legs, even though below-cloud measurements at a particular longitude could be separated by 500 m in altitude and more than 3 h in time. On average, pre-cloud aerosol can be represented by low altitude samples collected at the same longitude.

There were 3 intercomparison flights between the G-1 and C130, BAe-146 and Twin Otter that yielded data on LWC and CDNC (from a CDP or CAS probe). Results are summarized in Table 2. Intercomparisons were conducted with a several minute time separation between aircraft. Small differences in location, especially altitude, had a large influence on LWC. More significant are differences in CDNC where the G-1 values have to be reduced by 10, 17 and 38 % to match the C130, TO, and BAe146, respectively. Although the comparison with the BAe146 is based on a short sample through broken clouds, a particle balance between below cloud and in-cloud is consistent with the G-1 CDNC being approximately 20 % too high – of the same order as published estimates of measurement uncertainty (Fountoukis et al., 2007). This factor also agrees with inter-platform differences in CDNC vs. longitude (not shown).

ACPD
11, 17289–17336, 2011

3 Results

Source regions for aerosol and trace gases have been analyzed by Allen et al. (2011) and Bretherton et al. (2010) by means of back trajectories calculated for the marine boundary layer (MBL) at 950 hPa and free troposphere (FT) at 850 hPa starting from 20° S at distances from the shore varying from 70.5° W to 90° W. Much of this work is pertinent to the longitudinal and vertical pollutant distribution measured by the G-1. Allen et al. (2011) and Bretherton et al. (2010) found that pollutants in the near coastal MBL could be explained by low altitude winds from the S and SE that intersected the Chilean coast. Trajectories terminating further offshore where pollution levels are lower tend to remain off shore, missing coastal emission sources. FT back trajectories were more diverse. In one population, descending air from the direction of Australia and South Asia carried pollutants to the VOCALS region. Another category of FT trajectory prevalent between the coast and 75° W were northerlies from Peruvian coastal regions. A contribution to the FT consisting of return coastal flow from the MBL is hypothesized by Allen et al. (2011) based on instances with high humidity and low O_3.

3.1 Spatial distributions

Data have been segregated into marine boundary layer, pre-cloud, in-cloud, and free tropospheric subsets as defined in Table 3. Pre-cloud aerosol is an approximation to the aerosol actually ingested into a cloud, justified by observations such as presented in Fig. 3. Clouds were located primarily between 800 and 1200 m altitude with cloud base and inversion height increasing with distance from the shore (Rahn and Garreaud, 2010; Bretherton et al., 2010).

Figure 4 shows frequency distributions of sub-micrometer aerosol number and volume concentration and CO and O_3 mixing ratio as a function of longitude for the below cloud layer. Aerosol number concentration and volume decrease 2.3 and 3.6-fold, respectively between 70° and 75° W, the difference between number and volume appearing in the aerosol size distributions, presented below. There is a monotonic decrease in

ACPD
11, 17289–17336, 2011

CO between 70° and 75° W totaling 10 ppb, while O_3 increases by 9 ppb and continues to increase west of 75° to the limit of our sampling at 78° W. In contrast, CO and aerosol number and volume do not have a significant zonal gradient west of 75°. Median concentrations in the free troposphere are also given in Fig. 4. Concentrations are highest near the coast except for O_3. Relative to the marine boundary layer, CO and especially O_3 have a greater concentration in the free troposphere. Particle volume decreases several-fold with altitude but number concentration decreases only marginally, a result consistent with size distributions shown in a following section.

Even though the sampling region of the G-1 was primarily north of the 20° S corridor reported on by Allen et al. (2011), there is excellent agreement in longitudinal structure in the MBL and FT for the 3 quantities that can be directly compared: O_3, CO, and CN (albeit with a 15 nm lower size limit in the present study). SO_2 concentrations were below our detection limit of ~ 0.2 ppb except for a few near coast measurements, not surprising in a cloud covered MBL where there is opportunity for aqueous phase reaction with H_2O_2. With a more sensitive instrument, Allen et al. (2011) report mean SO_2 concentrations of 20–30 ppt, with higher values near the coast and concentrations approaching 1/2 ppb in a few discrete layers at 2–3 km altitude.

Frequency distributions as a function of altitude have been constructed by dividing the data set into altitude bins as shown in Fig. 5. Data points in and out of clouds are included for CO and O_3, but points with LWC > 0.01 g m^{-3} are excluded for aerosol number and volume. Because samples are not uniformly distributed in longitude or altitude, there are biases in constructing these vertical profiles. As can be seen from Fig. 1, high altitude points are primarily east of 74°. Also, according to Fig. 5f, data points between 400–800 m are closer to the shore than those in the lower altitude bin (100–400 m) thereby accounting for aerosol volume increasing with altitude in the two below cloud bins (Fig. 5b). The vertical structure shown in Fig. 4, in general, appears more pronounced than that shown in Fig. 5. This is partly an artifact caused by sampling inhomogeneities mentioned above. There is also a real difference in the data sets as the FT data in Fig. 4 incorporates the requirement that potential temperature,

ACPD
11, 17289–17336, 2011

θ, exceed 22 °C, a constraint that insures separation between below and above cloud aerosol size spectra.

Figure 5e shows that in each of the three above cloud altitude bins, dew point varies by about 40 °C, indicating that at a given altitude in the FT air masses with very different histories are being sampled. As dew point is controlled by the maximum altitude to which an air parcel is lifted, lower dew points indicate air masses that subsided from the middle or upper troposphere, whilst higher dew points indicate air masses that have a boundary layer origin. The association between dew point and air mass origin prompts us to examine aerosol and trace gas concentration as a function of dew point in Fig. 6. A qualitative correspondence between layers defined according to dew point and those defined according to altitude is that the below-cloud part of the MBL corresponds to the two bins with highest dew point (> 10 °C), the cloud layer has dew point between 6 and 10 °C, and the three above cloud layers are represented by three dew point ranges between 6 and −40 °C.

For soluble substances with a surface source, the decrease in temperature and specific humidity with altitude is an effective cold trap preventing upward transport and leading to a qualitative proportionality between accumulation mode aerosol and water vapor (Kleinman and Daum, 1991). Aerosol volume decreases with dew point, in this case by a factor of 6, due to precipitation removal of particles large enough to act as CCN whilst insoluble substances such as CO and O_3 are not affected. Particle number concentration does not decrease to the same extent because most of the particles in dry air are too small to act as CCN. Trends in the number concentration of larger particles, say $D_p > 0.1$ µm, more nearly follow aerosol volume.

Ozone is seen to increase in drier air as expected for a gas with an upper atmospheric source. Also contributing to the O_3 gradient is surface deposition and photochemical destruction by $O_3 + h\nu \rightarrow O(^1D)$; $O(^1D) + H_2O \rightarrow 2OH$, which proceeds more rapidly in moist air near the surface (Ayers et al., 1992). Given a long enough residence time, near surface O_3 concentrations can approach zero as seen by Kley et al. (1996) in the remote Pacific. Although photochemical destruction of O_3 in the MBL is

ACPD
11, 17289–17336, 2011

expected, concentrations in the limited geographic area covered by the G-1 increase with distance from the coast. The VOCALS region, unlike the remote Pacific, is characterized by strong subsidence and it is likely that the source of O_3 in the MBL towards the west is subsidence from the FT. Indeed, O_3 from the FT is used as an inert tracer to quantify cloud top entrainment (e.g., Faloona et al., 2005). Aerosol particles will be entrained as a component of FT O_3 containing air. Although large particles in the FT are fewer than in the MBL (Sect. 3.2, following), they can, as shown by Clarke et al. (1996, 1997), provide CCN to replace those lost by drizzle – a process of particular importance in the drizzled out POC regions further west than the G-1 sampled (Wood et al., 2011).

In the MBL, CO is anti-correlated with O_3 consistent with the oppositely directed east-west trends shown in Fig. 4c,d. Emission sources are located on land which lends some logic to CO concentrations being highest near the shore but does not address the near-shore O_3 which not only is low but is also anticorrelated with CO. CO–O_3 anticorrelations of the type observed in winter by Parrish et al. (1998) do not seem relevant in the low NO_x VOCALS region. Allen et al. (2011) suggest the possible effects of fresh emissions but also note that a transport process may be responsible. An explanation for the low near-shore O_3 may have to await process analysis of CTM results.

The anti-correlation between CO and O_3 disappears at the 0 to −20 °C dew point level and in the driest air is replaced with a significant positive correlation due to long range transport of pollution plumes. An extreme example occurred on Flight 081025a and is identified on Fig. 7. The polluted layer was at 74.5° W between 2300 and 2500 m altitude. Dew point at −40 °C was among the driest observed. Insoluble pollutants, CO and O_3 averaged 115 and 83 ppb, the highest levels observed during the campaign. Aerosol number and volume were several-fold less than at lower altitude but were the highest values observed in such dry air. Ten day back trajectories generated from the HYSPLIT model (Draxler and Rolph, 2010) descend from high altitude (> 7000 m) over the Pacific but are inconclusive regarding the origin of this air mass. As CO definitely

ACPD
11, 17289–17336, 2011

has a boundary layer source, these descending air parcels maintain a chemical record of a prior boundary layer residence.

In order not to distort statistical relations by a single high concentration plume, correlations for data with dew point between −20 and −40 °C have been calculated with and without data from 25 October. With the 25 October plume, a reduced major axis least squares regression yields a CO to O_3 ratio of 1.0 with an r^2 of 0.68. Removing the 25 October data yields a CO to O_3 ratio of 1.2 with an r^2 of 0.41. Both values indicate very efficient O_3 production and/or loss of O_3 in transport as compared with surface observations that have a CO/O_3 ratio a factor of 3 lower (Parrish et al., 1998). The 25 October plume shows up in the concentrations of aerosol sulfate and even more in organic aerosol (Fig. 7). A linear regression between organic aerosol and CO gives a ratio of 7.2 $\mu g\,m^{-3}\,ppm^{-1}$ CO ($r^2 = 0.56$). A similar ratio of 6.9 $\mu g\,m^{-3}\,ppm^{-1}$ CO is obtained without data from 25 October. These values are an order of magnitude lower than found in polluted boundary layer air masses after about one day of photochemical processing (Kleinman et al., 2008), indicating precipitation removal of aerosol.

In addition to the CO plumes observed in the driest air there are observations of high CO (> 80 ppb) concentration, located over a range of altitudes with dew points between 0 and 6 °C (i.e. in the bin just above the cloud layer). CO in these cases is anti-correlated with O_3. HYSPLIT back trajectories intercept or come close to the Peruvian coast in agreement with wind measurements presented by Bretherton et al. (2010) and Rahn and Garreaud (2010). Bretherton et al. (2010) note that heating of the Andean slope mixes moisture into a layer that becomes the lower free troposphere when advected over the Pacific. High concentrations of CO in the moist above cloud layer are further evidence of the upward mixing of continental boundary layer air. The next driest bin in Fig. 6 also has data points with high CO. Here the anti-correlation between CO and O_3 has changed into a lack of correlation.

Concentrations of aerosol sulfate and organics both decrease with altitude (Lee et al., 2011) or dew point (Fig. 7). There is a selective reduction in aerosol sulfate in dry air which could reflect a greater solubility and propensity for wet removal, relative

ACPD
11, 17289–17336, 2011

to organics, and/or a different mixture of sources affecting boundary layer and free tropospheric air. Whereas the organic to sulfate ratio is ∼0.1 in the marine boundary layer it increases to above 0.5 in the driest air and is greater than 1 in the plume encountered on 25 October. Absorption measurements were examined for information on light absorbing carbon aerosol. Except for isolated plumes and areas near land, aerosol absorption was too low to reliably quantify with a median value of 0.6 M m^{-1} in the boundary layer and 0.4 M m^{-1} above.

3.2 Aerosol size distribution

Aerosol size distributions measured with the SMPS are shown as a function of longitude in Fig. 8 for the below cloud layer and free troposphere. Below cloud aerosol has a characteristic two mode structure separated by a minimum. As described by Hoppel et al. (1986) this minimum is the result of a selective activation of larger aerosol particles in the cloud forming process. Aqueous phase chemistry, principally the oxidation of SO_2 to sulfate adds solute mass. Upon cloud evaporation larger aerosol particles are returned to the gas phase creating a mode (sometimes called a droplet mode) that is distinct from the smaller aerosol particles that have not increased in mass by aqueous phase chemistry. Composition measurements reported by Lee et al. (2011) show that sub micron size aerosol is primarily partially neutralized H_2SO_4, consistent with a formation route by aqueous phase oxidation of SO_2. It would be expected that the droplet mode contains a higher ratio of sulfate to organics than the Aitken mode. This, however, could not be tested using AMS size distributions because the volume of the Aitken mode was too small to quantify. With increasing distance from the shore, Fig. 8 shows that the droplet mode contains an increasing fraction of the total aerosol. At the same time, the droplet mode becomes narrower with a decreasing proportion of larger particle ($D_p > 300$ nm). The droplet mode size is nearly invariant ($D_p = 160$–185 nm) but the Hoppel minimum diameter and the Aitken mode size move to lower values. In contrast, free tropospheric aerosol is predominately unimodal with a mode size between that for Aitken and accumulation modes observed in the MBL.

ACPD
11, 17289–17336, 2011

Size distributions of aerosol particles as functions of dew point are shown in Fig. 9. Particles in the boundary/cloudy layer with $T_d > 6\,^{\circ}C$ are seen to have a bimodal distribution characteristic of cloud processing. Layers with dew point between −20 and 6 °C have on average a broad size distribution centered at 80–100 nm Most often, the individual size distributions are close to unimodal but when compared with a single log normal fit, have tails at large and small diameter. Though the apparent widths in the dry subsets shown in Fig. 9 are in part due to averaging over samples with different mode diameters between ∼40 and 110 nm, the individual distributions are wide with a median geometric standard deviation of 1.81. At the lowest dew points there are an increasing number of samples with an additional smaller, nucleation mode, not fully resolved by the SMPS. As a consequence, the average aerosol size becomes smaller.

3.3 First indirect effect

In Fig. 10, pre-cloud aerosol (Table 3) with $D_p > 100$ nm are compared with CDNC. As discussed below, 100 nm is a representative critical diameter for activation given composition, size spectra, and updraft velocity. Cloud droplet concentrations have been multiplied by 0.8 which brings the G-1 measurements into better agreement with the intercomparison data given in Table 2. An increase in CDNC with aerosol as shown in Fig. 10 is a necessary condition for the first indirect effect but as others have noted it is more difficult to make an association with brighter clouds. It can be seen that additional aerosol results in a less than proportionate increase in cloud droplets, a result that has been observed by many groups (e.g., Ramanathan, 2001; Twohy, 2005).

3.4 In-cloud aerosol

The number concentration of interstitial aerosol, N_{int}, can be estimated from a number balance between below and in-cloud particles, illustrated by the green arrow in Fig. 10. The fraction of in-cloud particles that are interstitial, defined using average values in the expression $(N_{int}/(N_{int} + \mathrm{CDNC}))$, is 0.27. Alternately, N_{int} can be obtained directly from

ACPD
11, 17289–17336, 2011

in-cloud aerosol measurements, but results will be biased high from shattered cloud droplets counted as aerosol particles. Despite this shortcoming, interstitial aerosol will be discussed using the later approach because co-located cloud and aerosol measurements allows a connection to be made with cloud microphysics. In-situ data for N_{int} includes broken clouds which leads to a further increase relative to data in Fig. 10.

Most clouds contained significant numbers of interstitial aerosol particles. This can be seen from the number balance in Fig. 10 for $N_{int} > 200\,cm^{-3}$ and from in-cloud observations in Fig. 11 in which average size spectra from the inside-cabin PCASP are given as a function of cloud liquid water content. Comparison is made to an average size distribution determined in cloud free air located along the same 102 constant altitude transects used for the cloud data. Although individual transects may not have cloud free portions, on average cloud free aerosol is nearly identical to pre-cloud aerosol defined in Table 3. Aerosol and LWC data are presented in Fig. 11 at 1 s time resolution, equivalent to an average over 100 m distance. Data from the in-cabin PCASP is available at 10 Hz but the added time resolution is defeated by uncertainties in sampling time and poor counting statistics. As shown below and as demonstrated in other measurement campaigns (e.g., Gerber et al., 2005) there is significant cloud structure including holes at smaller spatial scales. For the purpose of interpreting Fig. 11, sub 1 s structure effects results to the extent that the PCASP spectra are assigned to an incorrect LWC category. In particular, aerosol in short duration holes appear as a contribution to N_{int} at a LWC determined by a 1 s average.

Figure 11 shows a monotonic decrease in interstitial aerosol as cloud liquid water is increased. For clouds with LWC $> 0.1\,g\,m^{-3}$, the fraction of aerosol not activated changes from 47 % to 26 % as LWC is increased to above $0.6\,g\,m^{-3}$. The fraction of aerosol that is interstitial decreases markedly at large diameter, as has been found in multiple studies (e.g., Gillani et al., 1995).

Cloud droplet shatter contributes to N_{int}. In-cloud SMPS size spectra show extremely high concentrations of small particles, i.e. 10^3 to more than 10^4 particles cm^{-3} smaller than 50 nm diameter. Similar concentrations of small particles in-cloud have been

ACPD
11, 17289–17336, 2011

previously observed and attributed to droplet shatter (e.g., Hudson and Frisbie, 1991; Clarke et al., 1997; Weber et al., 1998). Given extremely high concentrations of small particles due to droplet shatter, the much less numerous accumulation mode aerosol do not stand out. Rather, they appear as a shoulder or sometimes a bump in the size distribution that is quantifiable as a separate mode by fitting the distribution to a sum of log normals, as illustrated in Fig. 12. In this case, a small percentage of in-cloud particles large enough to be detected by the PCASP are part of a tail on the shatter distribution and the majority appear to be part of a mode that is distinct from the shatter size distribution. According to the fitted log normals for 102 cloud transects, the shatter mode within the PCASP size range can vary between zero and several 10's of percent of the accumulation mode, with very few occurrences of particles as large as 200 nm. Although, the log normal fits are suggestive, there is no a priori reason why cloud droplet shatter should have this functional form, which leaves in doubt the quantitative apportionment of larger particles between droplet shatter and interstitial aerosol.

Both in and out of cloud, the number of particles larger than 600 nm is small. There is no evidence that the inside PCASP (or SMPS) is detecting partially evaporated cloud droplets in contrast to what has been observed for particles with $D_p > 400$–500 nm, measured outside of the cabin (Leaitch et al., 1996). The absence of these particles inside the cabin is a consequence of cloud droplets being too large to go through the aerosol inlet. Extra drying, beyond that supplied by a deicing heater, due to adiabatic compression and cabin heat also contributes. Size distribution measurements from the nose mounted PCASP, in contrast show a population of in-cloud particles with $D_p > 500$ nm that can be more numerous than the sub 500 nm population.

Interstitial aerosol representing evaporated cloud droplets or aerosol particles that did not activate were anti-correlated with CDNC in all clouds sampled by the G-1. Similar observations have been made by others (e.g., Gultepe et al., 1996). As a representative example we consider a case study cloud observed on Flight 081028a, centered at 75.2° W (Fig. 2). Figure 13a shows a 1 Hz time series of CDNC and N_{int} measured

ACPD
11, 17289–17336, 2011

with the CAS and inside-cabin PCASP, respectively. There are multiple spikes lasting no more than 1 s in which a decrease in CDNC is accompanied by an increase in N_{int}. There are also variations on time scales of tens of seconds or longer in which the relation between CDNC and N_{int} is less apparent.

A plot of CDNC vs. N_{int} (Fig. 13b) shows an overall anti-correlation but with considerable scatter. The anti-correlation that is apparent in the high frequency spikes in Fig. 13a is partially obscured by changes in pre-cloud aerosol and/or cloud dynamics that are important over spatial scales of order 5 km and greater. In order to account for the non-uniformity of the cloud, we qualitatively separate low and high frequency components. A 400 s binomial filter, subjectively selected, has been applied, yielding low frequency components shown by red lines in Fig. 13a. High frequency components called anomalies to avoid confusion with 10 Hz data presented later on are defined as the difference between a 1 Hz signal and the corresponding low frequency filtered component. A graph of high frequency anomalies in Fig. 13c has reduced scatter.

Low frequency changes in aerosol and cloud droplets contribute to scatter in Fig. 13b. Cloud regions which have different aerosol inputs or different dynamics can have CDNC vs. aerosol plots that are shifted relative to each other. In Fig. 13d, the original 1 s data has been subject to a 10 s running box car average, which is a visual aid to picking out contiguous points. Lines are drawn between consecutive data points and color coded to correspond to the time sequence in Fig. 13a. One can pick out 4 or 5 strands that represent contiguous cloud portions up to 10 km in length that individually show an anti-correlation between CDNC and N_{int}. Among the 102 clouds transects, this type of structure is common. At a still larger spatial scale approaching the length of the transect, CDNC and N_{int} are correlated (Fig. 13e). Depending on mesoscale structure, the low frequency changes in CDNC and N_{int} can be correlated, anti-correlated, or scattered.

Higher frequency measurements are useful in interpreting the presence of interstitial aerosol. Increasing the time response of cloud droplet measurements to 10 Hz as in Fig. 14, shows that the cloud contains regions in which CDNC decreases to near zero

ACPD
11, 17289–17336, 2011

accompanied by large decreases in LWC but relatively small changes in volume mean radius. It is expected that the interstitial aerosol shows similar high frequency structure but this is not observable with our sampling line.

A regression between the high frequency components of CDNC and accumulation mode aerosols has a slope of −2.0 for the case study cloud in Figs. 13 and 14, approximately equal to the median slope of −2.1 found for the entire data set of 102 clouds. Several factors contribute to the slope being steeper than minus 1, the value that would be obtained if removal of a single cloud droplet resulted in the appearance of an interstitial aerosol particle detected by the PCASP. First is the possibility of an overestimate in CDNC as suspected from the intercomparison data in Table 2. If actual CDNC are 80 % of measured, correcting the CDNC changes the slope by a factor of 0.8 (i.e. from −2 to −1.6). Second, cloud droplets could be formed from aerosol particles smaller than the 110 nm lower limit of detection of the PCASP. Sub-cloud aerosol size distributions have a Hoppel minimum at ∼ 75 nm, indicating that sometime in the air mass history, particles of that size were CCN (Cantrell et al., 1999). Third, and likely most important, is a degraded time response due to mixing in the inlet manifold leading to the inside-cabin PCASP. This effect has been simulated by constructing a PCASP signal which is the negative of CDNC, then subjecting it to 3 point binomial smoothing to simulate mixing. The resulting regression slope between the high frequency components of CDNC and the synthetic PCASP signal was −1.49, instead of −1 before smoothing. Results depend on the degree of smoothing and our choice is meant to be only illustrative. Supporting evidence for the importance of time response comes from the PCASP mounted on the aircraft nose which yields a median slope of −1.35.

ACPD
11, 17289–17336, 2011

4 Discussion

4.1 First indirect effect

Cloud reflectivity is dependent on many processes, the relation between cloud droplets and aerosol (Fig. 10) being only one component. More important to reflectivity is cloud liquid water path or, given a fixed cloud depth, liquid water content (Schwartz and Slingo, 1996). Measurements during VOCALS along 20° S from ∼72 to 86° W indicate that the westward decrease in aerosol concentration is accompanied by an increase in cloud depth and liquid water path (Allen et al., 2011; Bretherton et al., 2010) so that changes in reflectivity seen from satellites have to be apportioned between dynamical effects and aerosol perturbations, leaving aside the possibility that the two effects are coupled (Stevens and Feingold, 2009). An example of dynamical and aerosol effects operating in different directions is provided by our case study cloud. In that case interstitial aerosol decreases with westward distance in agreement with trends observed for below-cloud aerosol (Figs. 3 and 4a). By itself the decrease in aerosol is expected to lead to fewer but larger cloud droplets and a less reflective cloud towards the west. However, Fig. 14b,c shows an abrupt increase in cloud liquid water content and droplet size that presumably has a dynamic origin, positioned such that the dimming effect caused by fewer aerosol particles is opposed by a cloud brightening (dependent on cloud depth variations) caused by increased liquid water.

4.2 Interstitial aerosol

Our primary evidence that a substantial fraction of particles measured in-cloud by the inside-cabin PCASP actually represent evaporated cloud droplets or aerosol particles that did not activate is that these particles are anti-correlated with CDNC. Secondary evidence is the below and in-cloud number budget (Fig. 10) and the in-cloud size distribution (Fig. 12). The case study cloud shown in Figs. 13 and 14 is representative in many ways, but as a single cloud is not meant to illustrate features resulting from the

ACPD
11, 17289–17336, 2011

natural range in adiabaticity, position relative to cloud top and bottom, aerosol concentration, LWC, drizzle, and mesoscale structure seen during VOCALS.

A common feature of most cloud transects is that N_{int} rarely approaches zero even in regions with high CDNC or high LWC, i.e., regions most likely to have a high updraft velocity and/or be close to adiabatic. At the highest aerosol concentrations this might be due to competition for liquid water during ascent. However, this phenomena also occurs at low aerosol concentration, as in the case illustrated in Fig. 13. Whereas the increase in N_{int} that coincides with a decrease in CDNC (Fig. 13a–d) has a physical interpretation, the "background" N_{int} is at odds with other observations. According to the in-cloud SPMS size distributions, part of the background is due to cloud droplet fragmentation. This part, however, does not appear to be large enough to bring the in-situ N_{int} measurements into agreement with those obtained from a comparison between below and in-cloud particle number concentration (Fig. 11). It appears that there is an additional, unidentified, artifact source of N_{int}.

Absent entrainment or other complications, a high activation fraction should follow from the combination of chemical composition, size distribution, and vertical velocity, w, observed during the VOCALS campaign. This supposition was evaluated via an adiabatic parcel model calculation (Robinson, 1984) initialized with the MBL average aerosol size distributions observed at 71–72 and 76–77 longitude, corresponding to relatively high and low concentrations, respectively. It was assumed that aerosol had the properties of $(NH_4)_2SO_4$, which in terms of hygroscopicity is a close approximation to the actual composition. Bretherton et al. (2010) report standard deviations of w centered on $0.4\,m\,s^{-1}$ for near shore cloud measurements from the C130, a value in agreement with literature results cited as "representative" of MBL clouds (Nenes et al., 2010 and references therein). At a vertical velocity of $0.4\,m\,s^{-1}$ the critical diameter for activation is calculated to be 110 and 85 nm for the high and low concentration aerosol environments, respectively. Air parcel calculations should take into account the range in w (i.e., the pdf as used by e.g., Snider and Brenguier, 2000; Snider et al., 2003) which brings in values lower (and higher) than the median, opening the way for some

ACPD
11, 17289–17336, 2011

large particles to remain unactivated. However as pointed out by Guibert et al. (2003) particles respond to the supersaturation existing along their trajectories and a very low vertical velocity at cloud base may not be persistent.

High concentrations of interstitial particles can be caused by low hygroscopicity. Organic coating and kinetic limitations have been discussed in the literature as ways of slowing down the activation process (Chuang et al., 1997; Nenes et al., 2001; Feingold and Chuang, 2002). Although these effects cannot be discounted we view them as unlikely due to the predominance of a single hygroscopic aerosol type, the domain over which kinetic effects are significant, and the low fraction of organic material.

Cloud top entrainment of dry air evaporates cloud droplets returning aerosol particles to the interstitial phase. Depending on the horizontal dimensions of the entrained air the time sequence of anti-correlated CDNC and N_{int} (Fig. 13a) will be more or less spiky as observed from a moving platform. We have shown 1 Hz and 10 Hz data but it is known that clouds are inhomogeneous on smaller scales. Cloud top entrainment of dry air in Sc sampled during DYCOMS II was observed to produce holes with an average width (short dimension) of 5 m. These holes are defined by having reduced LWC compared with non-hole background areas (Gerber et al., 2005). The occurrence of dry areas within a 1 s, 100 m sampling interval is a possible mechanism for generating an aerosol particle that is called interstitial because on a 100 m spatial scale it is in a cloud but actually resides in clear air. Another way of generating dry holes is through a circulation mechanism that causes variations in local cloud base height such that at low altitude where LWC is low there are more encounters with clear air and therefore a higher N_{int}. In agreement with the circulation mechanism, Wang et al. (2009) find altitude gradients in LWC, CDNC, and N_{int} in Sc during the MASE campaign that produce a result observed here, namely that interstitial aerosol decreases at high LWC (their Fig. 2d–f).

ACPD
11, 17289–17336, 2011

5 Conclusions

During the VOCALS-REx field campaign, the DOE G-1 covered a longitude range between Arica on the coast of Chile (70.3° W) and 78° W, an 800 km distance over which MODIS retrievals show a strong gradient in CDNC and effective radius. Aerosol number and volume concentration in the MBL decreased with off-shore distance with most of the decrease occurring between the coast and 75° W. This pattern is consistent with the trajectory analysis of Allen et al. (2011) and Bretherton et al. (2010) that indicate a source region to the south along the Chilean coast, whose impact is felt most often east of 75° W and with decreasing frequency further west. MBL concentrations of O_3 increase with distance from the coast while CO concentrations decrease indicating a nearby continental source for the latter.

Aerosol in the MBL is acidic sulfate with a 10–15 % admixture of organics consistent with emissions dominated by Cu smelters and power plants (Lee et al., 2011). MBL aerosol have an Aitken and accumulation mode with geometric mean diameters of 45–60 nm and 160–185 nm, respectively, separated by a Hoppel minimum. In the FT, number size distributions are unimodal and broad, centered at 90 nm.

In each of three altitude ranges, collectively spanning the FT from 1200 to 3000 m, dew point varied by more than 40 °C, showing that within a narrow altitude span, air masses with very different histories were sampled. The requirement that an ascending air mass has a relative humidity less than 100 %, combined with a strong dependence of temperature on altitude implies that the lowest dew point air observed (−40 °C) originated above 8 km altitude (assuming a surface temperature of 15 °C and a lapse rate of 6.5 °C km^{-1}). Conversely, moist air implies a low altitude source.

Frequency distributions of CO, O_3, aerosol number, and aerosol volume are provided as functions of altitude and dew point. Using dew point in place of altitude has the advantage of separating air masses according to history and highlights the different behavior of soluble and insoluble pollutants (Kleinman and Daum, 1991). Dew point more clearly picks up trends in O_3 because O_3 has a source in the dry upper atmosphere

ACPD
11, 17289–17336, 2011

and a MBL sink. There is a pronounced decrease in aerosol volume with dew point as low dew point air masses have been subject to cloud processes that have removed all but a few percent of their total water. Removed along with water are soluble substances such as accumulation mode particles that are CCN. The decrease with dew point of aerosol number concentration is less extreme because of the dominance of smaller less easily activated particles in the FT. The FT population of aerosol, however, does contain some accumulation mode size particles ($D_p > 100$ nm) which will subside into the MBL, much the same as O_3, thereby providing a source of CCN to replace that lost by drizzle (Clarke et al., 1996, 1997). Relative solubility may play a role in the 5 fold increase in the organic aerosol to sulfate ratio with decreasing dew point. It is also possible that the high ratio at low T_d reflects emission rates in areas not dominated by Cu smelters and power plants. Even with an elevated organic to sulfate ratio in dry air, the organic aerosol to CO ratio is an order of magnitude lower than observed in day old plumes in the boundary layer in other field studies.

One hundred and two constant altitude cloud transects were identified and used to examine relations between CDNC and the number concentration of interstitial aerosol (N_{int}) as measured by a heated PCASP inside the aircraft cabin. In each transect CDNC and N_{int} are anti-correlated, suggesting that a decrease in cloud droplets by e.g. mixing or evaporation leads to the appearance of interstitial aerosol. One cloud sampled over a 35 km transect was selected for a case study. Within this cloud there were 4 or 5 regions with distinctly different relations between CDNC and N_{int} contributing to scatter over the 35 km cloud. Much of the scatter could be removed by applying a high pass filter and examining the anomalies determined as the total signal less the low frequency variation.

Measurements from the inside-cabin PCASP indicate that between 1/4 (LWC > 0.6 g m^{-3}) and 1/2 (LWC = 0.1 to 0.2 g m^{-3}) of aerosol particles with $D_p > 110$ nm remain as interstitial during cloud transects. A comparison of pre-cloud air with CDNC yields an interstitial fraction of 1/4. Adiabatic parcel model calculations based on measured aerosol composition, concentration, size distribution, and a 0.4 cm s^{-1} vertical

ACPD
11, 17289–17336, 2011

velocity show that most aerosol in the PCASP size range should be activated. It is possible that a portion of the interstitial aerosol is derived from shattered cloud droplets or from an unknown artifact. Leaving aside measurement uncertainties there are several possible explanations, namely that some air parcels had less than average vertical velocities, particles were never activated, or that cloud droplets evaporated. Creation of dry holes by cloud top entrainment or a circulation mechanism that causes variations in local cloud base height need to be considered.

Acknowledgement. We thank chief pilot Bob Hannigan and the flight crew from PNNL for a job well done. We gratefully acknowledge the Atmospheric Science Program within the Office of Biological and Environmental Research of DOE for supporting field and analysis activities and for providing the G-1 aircraft. Use of a c-ToF-AMS provided by EMSL is appreciated. The VOCALS Regional Experiment owes its success to many people. We would like to single out Robert Woods (Univ. of Washington), Christopher Bretherton (Univ. of Washington), and C. Roberto Mechoso (UCLA) for their organizational skills and scientific leadership. S. S. Yum is partially supported by the Korean Meteorological Administration Research and Development Program under Grant RACS 2010-5001. This research was performed under sponsorship of the US DOE under contracts DE-AC02-98CH10886.

References

Allen, G., Coe, H., Clarke, A., Bretherton, C., Wood, R., Abel, S. J., Barrett, P., Brown, P., George, R., Freitag, S., McNaughton, C., Howell, S., Shank, L., Kapustin, V., Brekhovskikh, V., Kleinman, L., Lee, Y.-N., Springston, S., Toniazzo, T., Krejci, R., Fochesatto, J., Shaw, G., Krecl, P., Brooks, B., McMeeking, G., Bower, K. N., Williams, P. I., Crosier, J., Crawford, I., Connolly, P., Allan, J. D., Covert, D., Bandy, A. R., Russell, L. M., Trembath, J., Bart, M., McQuaid, J. B., Wang, J., and Chand, D.: South East Pacific atmospheric composition and variability sampled along 20° S during VOCALS-REx, Atmos. Chem. Phys., 11, 5237–5262, doi:10.5194/acp-11-5237-2011, 2011.

Ayers, G. P., Penkett, S. A., Gillett, R. W., Bandy, B., Galbally, I. E., Meyer, C. P., Elsworth, C. M., Bentley, S. T., and Forgan, B. W.: Evidence for photochemical control of ozone concentrations in unpolluted marine air, Nature, 360, 446–449, 1992.

ACPD
11, 17289–17336, 2011

Bretherton, C. S., Wood, R., George, R. C., Leon, D., Allen, G., and Zheng, X.: Southeast Pacific stratocumulus clouds, precipitation and boundary layer structure sampled along 20° S during VOCALS-REx, Atmos. Chem. Phys., 10, 10639–10654, doi:10.5194/acp-10-10639-2010, 2010.

Cantrell, W., Shaw, G., and Benner, R.: Cloud properties inferred from bimodal aerosol number distribution, J. Geophys. Res., 104, 27615–27624, 1999.

Chand, D., Hegg, D. A., Wood, R., Shaw, G. E., Wallace, D., and Covert, D. S.: Source attribution of climatically important aerosol properties measured at Paposo (Chile) during VOCALS, Atmos. Chem. Phys., 10, 10789–10801, doi:10.5194/acp-10-10789-2010, 2010.

Chuang, P. Y., Charlson, R. J., and Seinfeld, J. H.: Kinetic limitations on droplet formation in clouds, Nature, 390, 594–596, 1997.

Clarke, A. D., Li, Z., and Litchy, M.: Aerosol dynamics in the equatorial Pacific Marine boundary layer: microphysics, diurnal cycles and entrainment, Geophys. Res. Lett., 23, 773–736, 1996.

Clarke, A. D., Uehara, T., and Porter, J. N.: Atmospheric nuclei and related aerosol fields over the Atlantic: clean subsiding air and continental pollution during ASTEX, J. Geophys. Res., 102, 25281–25292, 1997.

Clegg, S. L. and Wexler, A. S.: Densities and apparent molar volumes of atmospherically important electrolyte solutions. 2. The system H^+-HSO_4^--SO_4^{2-}-H_2O from 0–3 mol kg^{-1} as a function of temperature and H^+-NH_4^+-HSO_4^--SO_4^{2-}-H_2O from 0–6 mol kg^{-1} at 25 °C using a Pitzer ion interaction model, and NH_4HSO_4-H_2O and $(NH_4)_3H(SO_4)_2$-H_2O over the entire concentration range, J. Phys. Chem. A 115, 3461–3474, 2011.

Clegg, S. L., Brimblecombe, P., and Wexler, A. S.: A thermodynamic model of the system H^+-NH_4^+-SO_4^{2-}-NO_3^--H_2O at tropospheric temperatures, J. Phys. Chem. A, 102, 2137–2154, 1998.

Collins, D. R., Flagan, R. C., and Seinfeld, J. H.: Improved inversion of scanning DMA data, Aerosol Sci. Technol., 36(1), 1–9, 2002.

Draxler, R. R. and Rolph, G. D.: HYSPLIT (HYbrid Single-Particle Lagrangian Integrated Trajectory) Model access via NOAA ARL READY Website, available at: http://ready.arl.noaa.gov/HYSPLIT.php (last access: January 2011), NOAA Air Resources Laboratory, Silver Spring, MD, 2010.

Faloona, I., Lenschow, D. H., Campos, T., Stevens, B., van Zanten, M., Blomquist, B., Thornton, D., Bandy, A., and Gerber, H.: Observations of entrainment in Eastern Pacific marine

ACPD
11, 17289–17336, 2011

stratocumulus using three conserved scalers, J. Atmos. Sci., 62, 3268–3285, 2005.
Feingold, G. and Chuang, P. Y.: Analysis of the influence of film-forming compounds on droplet growth: implications for cloud microphysical processes and climate, J. Atmos. Sci., 59, 2006–2018, 2002.
Fountoukis, C., Nenes, A., Meskhidze, N., Bahreini, R., Conant, W. C., Jonsson, H., Murphy, S., Sorooshian, A., Varutbangkul, V., Brechtel, F., Flagan, R. C., and Seinfeld, J. H.: Aerosol-cloud drop concentration closure for clouds sampled during the Intercontinental Consortium for Atmospheric Research on Transport and Transformation 2004 campaign, J. Geophys. Res., 112, D10S30, doi:10.1029/2006JD007272, 2007.
Gerber, H., Arends, B. G., and Ackerman, A. S.: A new microphysics sensor for aircraft use, Atmos, Res., 31, 235–252, 1994.
Gerber, H., Frick, G., Malinowski, S. P., Brenguier, J.-L., and Burnet, F.: Holes and entrainment in stratocumulus, J. Atmos. Sci., 62, 443–459, 2005.
Gillani, N. V., Schwartz, S. E., Leaitch, W. R., Strapp, J. W., and Isaac, G. A.: Field observations in continental stratiform clouds: partitioning of cloud particles between droplets and unactivated interstitial aerosols, J. Geophys. Res., 100, 18687–18706, 1995.
Guibert, S., Snider, J. R., and Brenguier, J.-L.: Aerosol activation in marine stratocumulus clouds: 1. measurement validation for a closure study, J. Geophys. Res., 108, 8628, doi:10.1029/2002JD002678, 2003.
Gultepe, I., Isaac, G. A., Leaitch, W. R., and Banic, C. M.: Parameterizations of marine stratus microphysics based on in situ observations: implications for GCMs, J. Climate, 9, 345–357, 1996.
Haller, A. G., Strawa, A. W., Schmid, B., Andrews, E., Ogren, J., Sheridan, P., Ferrare, R., Covert, D., Elleman, R., Jonsson, H., Bokarius, K., and Luu, A.: Atmospheric radiation measurements aerosol intensive operating period: comparison of aerosol scattering during coordinated flights, J. Geophys. Res., 111, D05S09, doi:10.1029/2005JD006250, 2006.
Hoppel, W. A., Frick, G. M., and Larson, R. E.: Effects of nonprecipitating clouds on the aerosol size distribution in the marine boundary layer, Geophys. Res. Lett., 13, 125–128, 1986.
Hudson, J. G. and Frisbie, P. R.: Cloud condensation nuclei near marine stratus, J. Geophys. Res., 96, 20795–20808, 1991.
Kleinman, L. I. and Daum, P. H.: Vertical distribution of aerosol particles, water vapor, and insoluble trace gases in convectively mixed air, J. Geophys. Res., 96, 991–1005, 1991.
Kleinman, L. I., Daum, P. H., Lee, Y.-N., Senum, G. I., Springston, S. R., Wang, J., Berkowitz, C.,

ACPD
11, 17289–17336, 2011

Hubbe, J., Zaveri, R. A., Brechtel, F. J., Jayne, J., Onasch, T. B., and Worsnop, D.: Aircraft observations of aerosol composition and ageing in New England and Mid-Atlantic States during the summer 2002 New England Air Quality Study field campaign, J. Geophys. Res., 112, D09310, doi:10.1029/2006JD007786, 2007.

Kleinman, L. I., Springston, S. R., Daum, P. H., Lee, Y.-N., Nunnermacker, L. J., Senum, G. I., Wang, J., Weinstein-Lloyd, J., Alexander, M. L., Hubbe, J., Ortega, J., Canagaratna, M. R., and Jayne, J.: The time evolution of aerosol composition over the Mexico City plateau, Atmos. Chem. Phys., 8, 1559–1575, doi:10.5194/acp-8-1559-2008, 2008.

Kley, D., Crutzen, P. J., Smit, H. G. J., Vömel, H., Oltmans, S. J., Grassl, H., and Ramamathan, V.: Observations of near-zero ozone concentrations over the convective Pacific: effects on air chemistry, Science, 274, 230–233, 2006.

Leaitch, W. R., Banic, C. M., Isaac, G. A., Couture, M. D., Liu, P. S. K., Gultepe, I., Li, S.-M., Kleinman, L. I., Daum, P. H., and MacPherson, J. I.: Physical and chemical observations in marine stratus during the 1993 North Atlantic Regional Experiment: factors controlling cloud droplet number concentrations, J. Geophys. Res., 101, 29123–29135, 1996.

Lee, Y.-N., Springston, S., Jayne, J., Wang, J., Senum, G., Hubbe, J., Alexander, L., Brioude, J., Spak, S., Mena-Carrasco, M., Kleinman, L., and Daum, P.: Aerosol composition, chemistry, and source characterization during the 2008 VOCALS Experiment, Atmos. Chem. Phys. Discuss., in preparation, 2011.

Liu, Y. and Daum, P. H.: The effect of refractive index on size distributions and light scattering coefficients derived from optical particle counters, J. Aerosol Sci., 8, 945–957, 2000.

Nenes, A., Ghan, S., Abdul-Razzak, H., Chuang, P. Y., and Seinfeld, J. H.: Kinetic limitations on cloud droplet formation and impact on cloud albedo, Tellus B, 53, 133–149, 2001.

Parrish, D. D., Trainer, M., Holloway, J. S., Yee, J. E., Warshawsky, M. S., Fehsenfeld, F. C., Forbes, G. L., and Mody, J. L.: Relationship between ozone and carbon monoxide at surface sites in the North Atlantic region, J. Geophys. Res., 103, 13357–13376, 1998.

Rahn, D. A. and Garreaud, R.: Marine boundary layer over the subtropical southeast Pacific during VOCALS-REx – Part 1: Mean structure and diurnal cycle, Atmos. Chem. Phys., 10, 4491–4506, doi:10.5194/acp-10-4491-2010, 2010.

Ramanathan, V., Crutzen, P. J., Kiehl, J. T., and Rosenfeld, D.: Aerosols, climate, and the hydrological cycle, Science, 294, 2119–2124, 2001.

Robinson, N. F.: The efficient numerical calculation of condensational cloud droplet growth, J. Atmos. Sci., 41, 698–700, 1984.

ACPD
11, 17289–17336, 2011

Schwartz, S. E. and Slingo, A.: Enhanced shortwave cloud radiative forcing due to anthropogenic aerosols, in: Clouds, Chemistry and Climate, Proceedings of NATO Advanced Research Workshop, Ringberg, Germany, 21–25 March 1994, edited by: Crutzen, P. and Ramanathan, V., Springer, Heildelberg, 191–236, 1996.

Snider, J. R. and Brenguier, J.-L.: Cloud condensation nuclei and cloud droplet measurements during ACE-2, Tellus B, 52, 828–842, 2000.

Snider, J. R., Guibert, S., Brenguier, J.-L., and Putard, J.-P.: Aerosol activation in marine stratocumulus clouds: 2. Köhler and parcel theory closure studies, J. Geophys. Res., 108, 8629, doi:10.1029/2002JD002692, 2003.

Stevens, B. and Feingold, G.: Untangling aerosol effects on clouds and precipitation in a buffered system, Nature, 461, 607–613, 2009.

Springston, S. R., Kleinman, L. I., Nunnermacker, L. J., Brechtel, F., Lee, Y.-N., and Wang, J.: Chemical evolution of an isolated power plant plume during the TexAQs 2000 study, Atmos. Environ., 39, 3431–3443, 2005.

Twohy, C. H., Petters, M. D., Snider, J. R., Stevens, B., Tahnk, W., Wetzel, M., Russell, L., and Burnet, F.: Evaluation of the aerosol indirect effect in marine stratocumulus clouds: droplet number, size, liquid water path, and radiative impact, J. Geophys. Res., 110, D08203, doi:10.1029/2004JD005116, 2005.

Wang, J., Daum, P. H., Yum, S. S., Liu, Y., Senum, G. I., Lu, M.-L., Seinfeld, J. H., and Jonsson, H.: Observations of marine stratocumulus microphysics and implications for processes controlling droplet spectra: Results from the Marine Stratus/Stratocumulus Experiment, J. Geophys. Res., 114, D18210, doi:10.1029/2008JD011035, 2009.

Weber, R. J., Clarke, A. D., Litchy, M., Li, J., Kok, G., Schillawski, R. D., and McMurry, P. H.: Spurious aerosol measurements when sampling from aircraft in the vicinity of clouds, J. Geophys. Res., 103, 28337–28346, 1998.

Wood, R., Bretherton, C., Huebert, B., Mechoso, C. R., and Weller, R.: VOCALS-SouthEast Pacific Regional Experiment (REx) Scientific Program Overview, available at: http://www.eol.ucar.edu/projects/vocals/documentation/vocals_overview.pdf (last access: January 2011), June 2007.

Wood, R., Mechoso, C. R., Bretherton, C. S., Weller, R. A., Huebert, B., Straneo, F., Albrecht, B. A., Coe, H., Allen, G., Vaughan, G., Daum, P., Fairall, C., Chand, D., Gallardo Klenner, L., Garreaud, R., Grados, C., Covert, D. S., Bates, T. S., Krejci, R., Russell, L. M., de Szoeke, S., Brewer, A., Yuter, S. E., Springston, S. R., Chaigneau, A., Toniazzo, T., Min-

ACPD
11, 17289–17336, 2011

nis, P., Palikonda, R., Abel, S. J., Brown, W. O. J., Williams, S., Fochesatto, J., Brioude, J., and Bower, K. N.: The VAMOS Ocean-Cloud-Atmosphere-Land Study Regional Experiment (VOCALS-REx): goals, platforms, and field operations, Atmos. Chem. Phys., 11, 627–654, doi:10.5194/acp-11-627-2011, 2011.

ACPD
11, 17289–17336, 2011

Table 1. Aerosol and cloud droplet instruments.

Instrument	Primary function	D_p range
CPC3025[1]	Total aerosol	> 3 nm
CPC3010[1]	Total aerosol	> 10 nm
SMPS (DMA)[2]	Aerosol mobility size spectra	15–440 nm
PCASP[3]	Cabin	0.11–3 µm
PCASP[3]	Pylon	0.11–3 µm
CAS	Cloud droplet	0.6–56 µm
CIP	Drizzle	8–940 µm
AMS	Aerosol composition	60–600 nm
PILS	Aerosol composition	< 2 µm

[1] DMT.
[2] TSI Inc., model 3081 DMA and model 3010 condensation particle counter.
[3] PCASP-100X (Particle Measuring Systems, Inc., Boulder, CO) with SPP-200 electronics (Droplet measurement Technologies. Boulder, CO).

ACPD
11, 17289–17336, 2011

Table 2. Cloud sampling intercomparisons.

Platform	Date	G-1			Other aircraft		
		CD	LWC	Time[1]	CD	LWC	Time[1]
TO	26 Oct	402	0.16	10:47–10:52	335	0.14	10:54–11:04
C130	4 Nov	226	0.10	11:28–11:35	203	0.16	11:25–11:33
BAe-146	12 Nov	47.3[2]	0.0065[2]	12:49–12:56	29.3	0.0095	12:45–15:51

[1] Rounded off to nearest minute.
[2] Maximum values $\sim 400\,cm^{-3}$, $0.1\,g\,m^{-3}$, in-cloud for ~ 1 min.

ACPD
11, 17289–17336, 2011

Table 3. Definition of atmospheric layers.

Variable[1]	Data subset			
	Marine boundary layer	Pre-cloud	In-cloud	Above-cloud
Altitude (m)	< 800	Below and within 15 km of cloud	> 600	> 1200
RH (%)	n/a	< 90	n/a	n/a
Theta (°C)	n/a	n/a	n/a	> 22
LWC ($g\,m^{-3}$)	< 0.01	< 0.01	> 0.02 $LWC_{avg} > 0.05$	< 0.01

[1] Condition applies to each 1 s time period within averaging time, except for LWC_{avg} which is an average value over a 1 min SMPS scan.

ACPD
11, 17289–17336, 2011

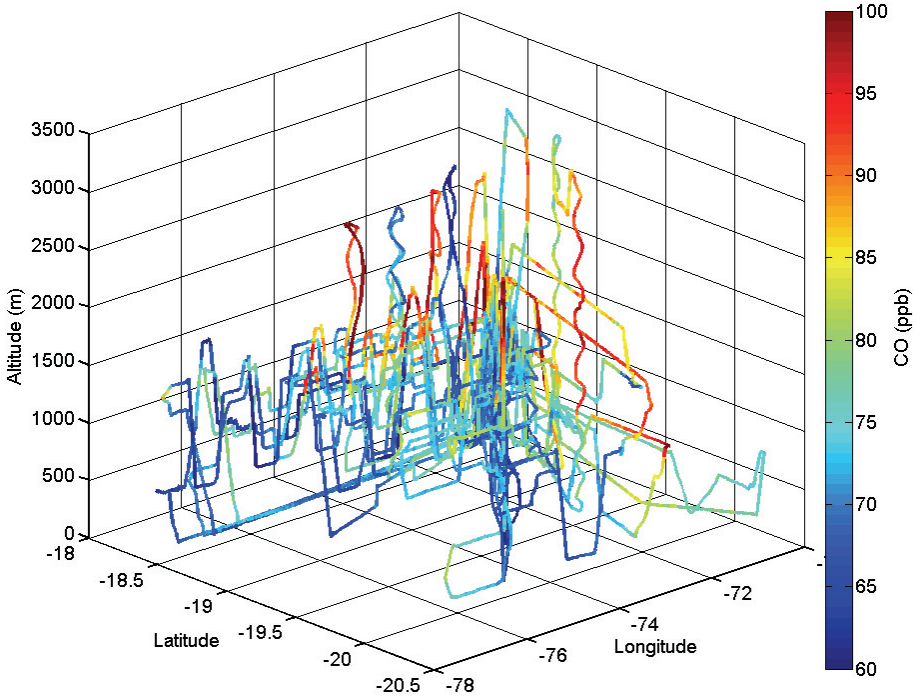

Fig. 1. Ground track of G-1 color coded by CO concentration. A portion of one flight south of −20.5 latitude not shown.

ACPD
11, 17289–17336, 2011

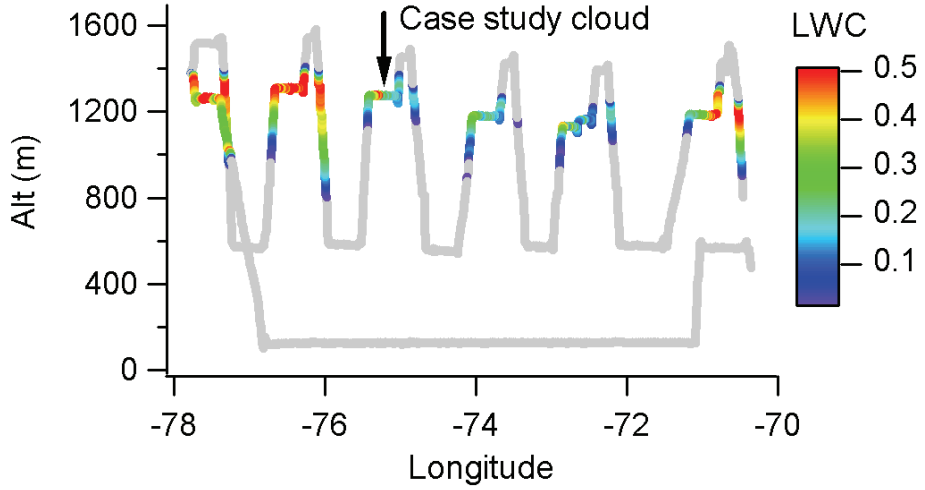

Fig. 2. Longitude–altitude cross section of flight track for 081028a color coded for cloud liquid water content in $g\,m^{-3}$. Cloud at −75.2° W longitude is used to illustrate anti-correlation between cloud droplets and interstitial aerosol.

ACPD
11, 17289–17336, 2011

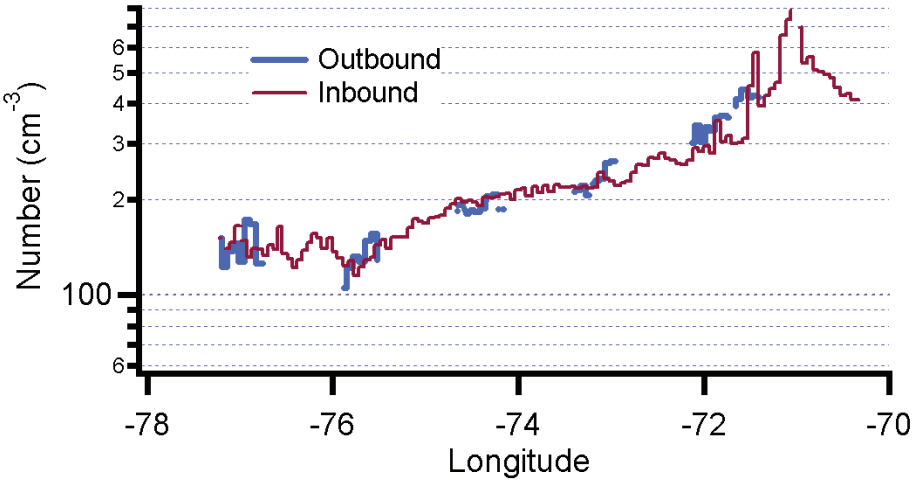

Fig. 3. Below cloud level SMPS measurement of number of particles with $D_p > 75$ nm.

ACPD
11, 17289–17336, 2011

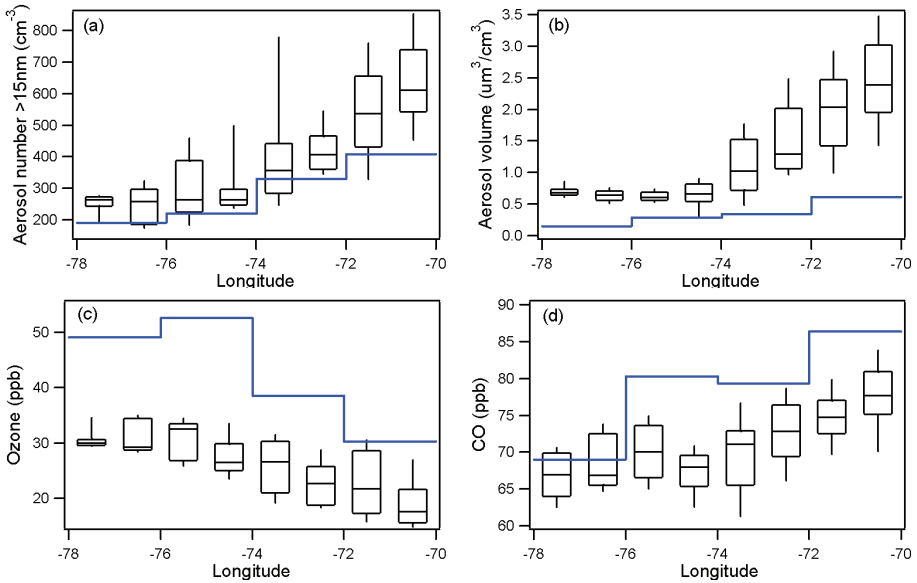

Fig. 4. Box plot showing frequency distribution of below cloud measurements of **(a)** aerosol number concentration and **(b)** volume measured by SMPS, **(c)** O_3, and **(d)** CO. Box indicates the 25th to 75th percentile range with line for median. Whiskers show 10th and 90th percentile values. Blue lines indicate the median values of FT observation divided into two degree longitude bins.

ACPD
11, 17289–17336, 2011

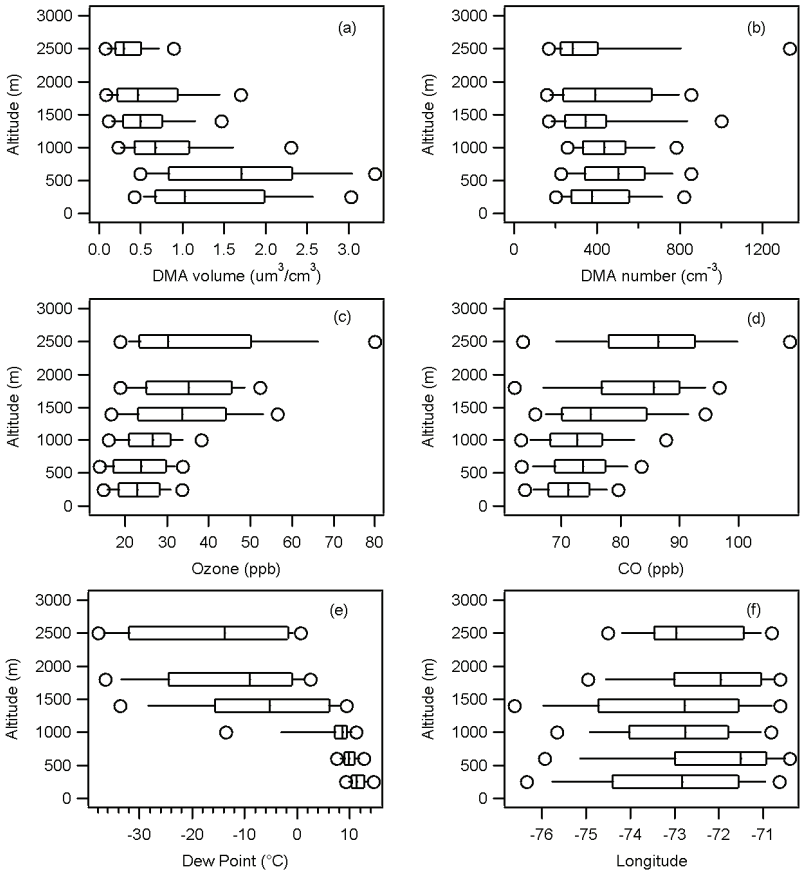

Fig. 5. Frequency distribution as a function of altitude. Box indicates the 25th to 75th percentile range with line for median. Whiskers show 10th and 90th percentile values. Circles are 5th and 95th percentile. Altitude bins are 100–400 m, 400–800 m, 800–1200 m, 1200–1600 m, 1600–2000 m, and above 2000 m.

ACPD
11, 17289–17336, 2011

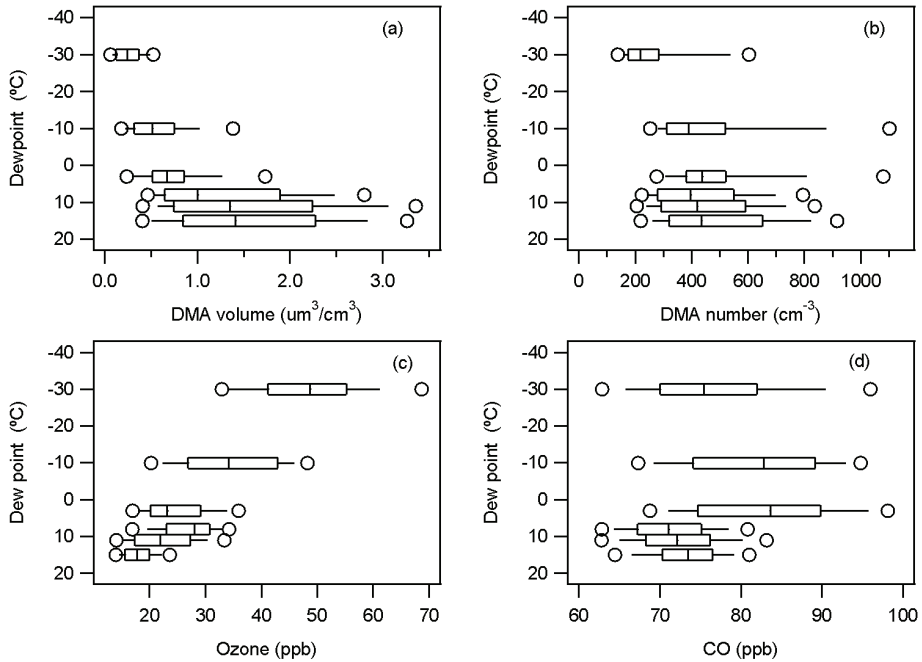

Fig. 6. Frequency distribution as a function of dew point. Box plot format same as in Fig. 5. Dew point bins are 16 to 12 °C, 12 to 10 °C, 10 to 6 °C, 6 to 0 °C, 0 to −20 °C, −20 to −40 °C. Qualitatively, the first 2 bins are below cloud, the third bin in the cloud layer, and the driest 3 bins above cloud.

ACPD
11, 17289–17336, 2011

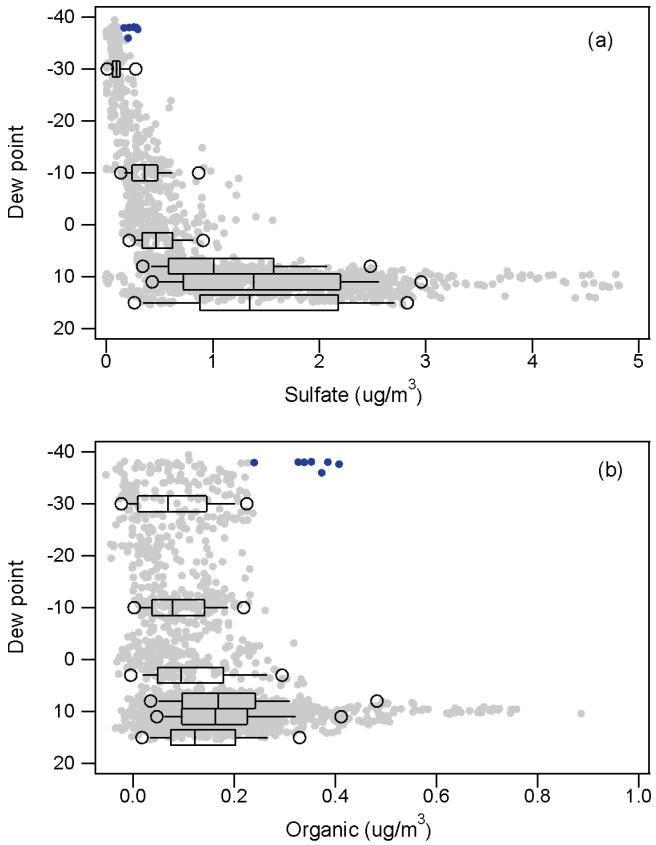

Fig. 7. Box plot showing frequency distributions for **(a)** sulfate and **(b)** organic aerosol measured with the AMS as a function of dew point. Box plot has same format as in Fig. 5. Each gray point represents data averaged over a DMA scan. Data points with LWC $> 0.01\,\mathrm{g\,m^{-3}}$ are excluded. Blue points are 7 min of measurements in an organic rich plume on 25 October.

ACPD
11, 17289–17336, 2011

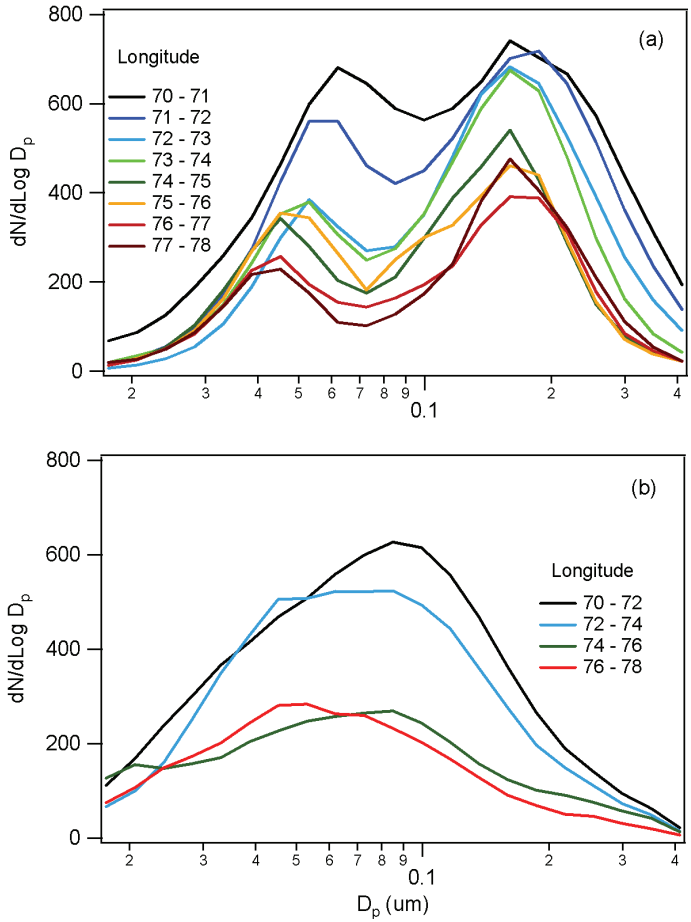

Fig. 8. Aerosol size distribution measured with SMPS **(a)** below cloud layer and **(b)** above cloud layer.

ACPD
11, 17289–17336, 2011

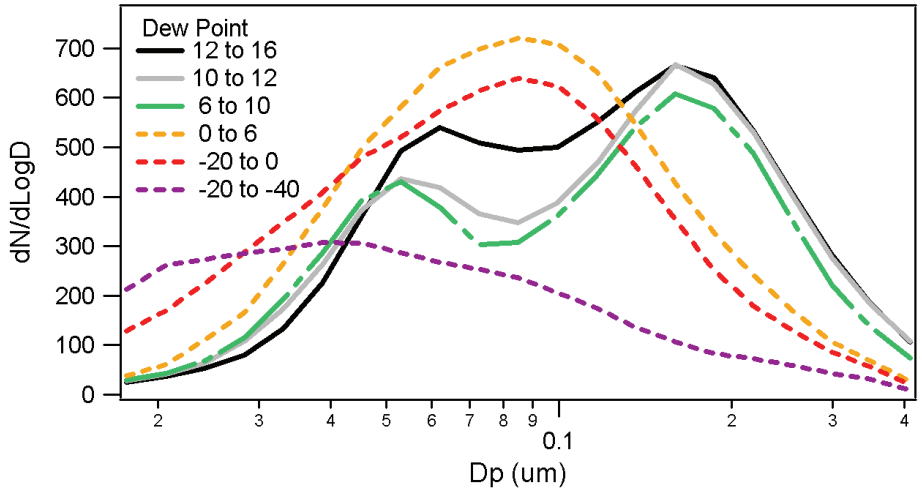

Fig. 9. Aerosol size distribution in cloud-free air from the SMPS as a function of dew point. Qualitatively, dew points from 10 to 16 °C are located below cloud, 6–10 °C is the cloud layer, and dew points below 6 °C are in the free troposphere, above cloud.

ACPD
11, 17289–17336, 2011

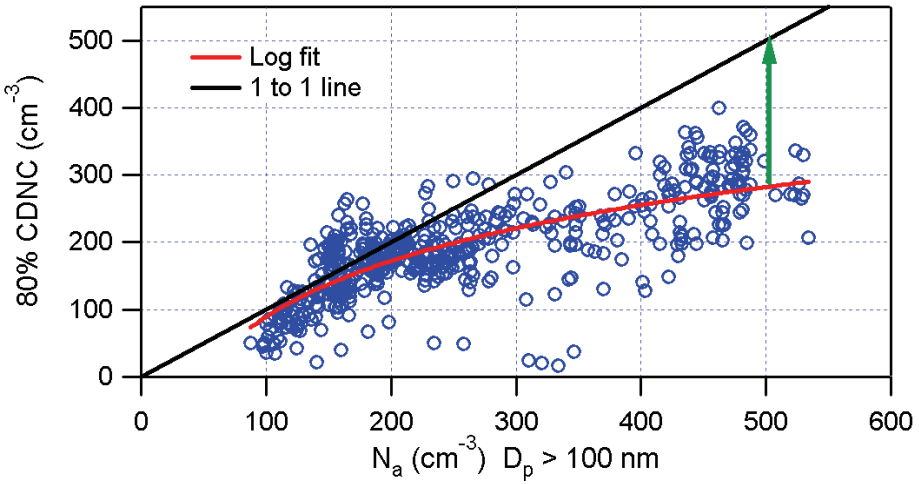

Fig. 10. Cloud droplet number concentration (CDNC) as a function of pre-cloud aerosol with $D_p > 100$ nm. Each data point is ~1 min of in-cloud data and an average of several minutes of aerosol data identified as pre-cloud. Broken clouds are eliminated. CDNC has been multiplied by 0.8. Equation of red line, after multiplying CDNC by 0.8, is $\text{CDNC} = -463 + 276\log_{10}(N_a)$. Data points above line are due to activation of aerosol smaller than 75 nm or imprecision in indentifying pre-cloud air. Green arrow illustrates number of interstitial aerosol with $D_p > 100$ nm that give number balance between below and in-cloud particles, placed at $N_a = 500\,\text{cm}^{-3}$ for illustration.

ACPD
11, 17289–17336, 2011

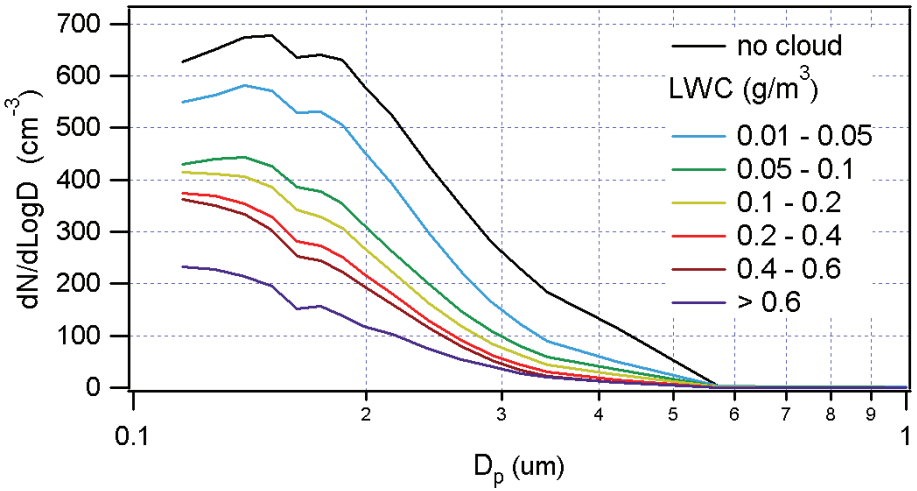

Fig. 11. Interstitial aerosol measured with in-cabin PCASP as a function of LWC. Reference "no-cloud" spectra is an average over all 1 s intervals on 102 cloud transects in which LWC < 0.01 g m^{-3}. PCASP size range extends to 3 µm but is indistinguishable from zero on a linear scale. The discontinuity at 160 nm is located at the intersection of two instrument ranges.

ACPD
11, 17289–17336, 2011

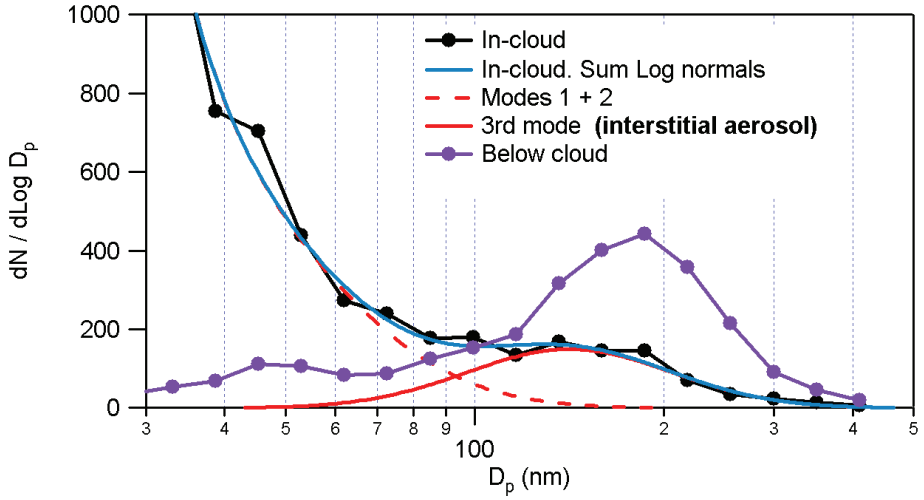

Fig. 12. In and below-cloud SMPS size distributions from the 28 October case study cloud. Black circles are in-cloud SMPS measurements which have been fit to a sum of 3 log normals (blue line). The 3rd mode is identified as interstitial aerosol. The dashed red line indicates the sum of the 2 smaller modes which in this case make a minor contribution to number concentration in the PCASP size range. For comparison the purple trace is below-cloud aerosol. Points in both SMPS size distributions are joined by straight lines for easy visualization.

ACPD
11, 17289–17336, 2011

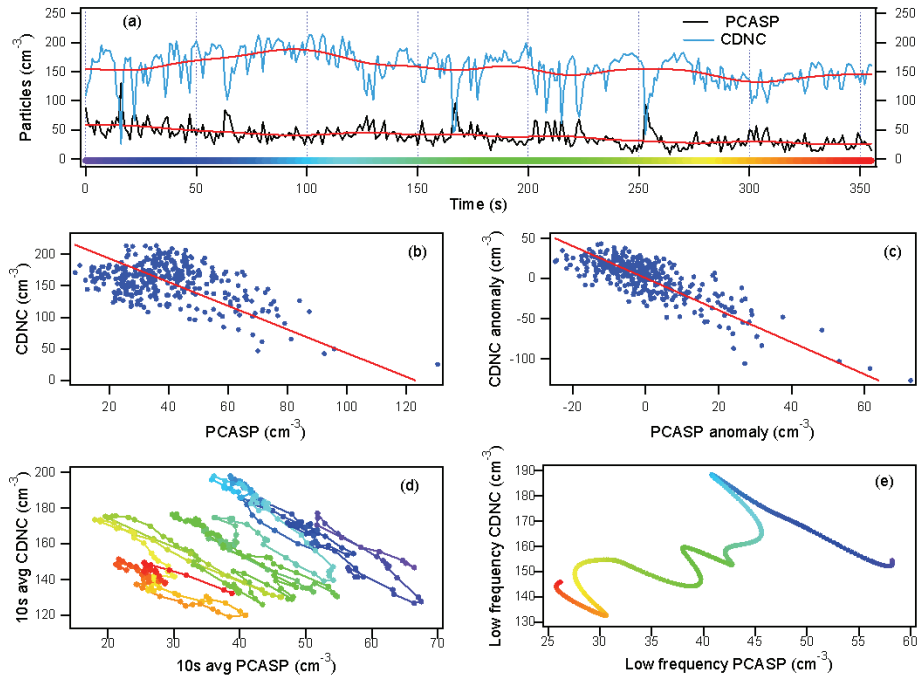

Fig. 13. Interstitial aerosol and cloud droplet number in cloud sampled on 28 October (see Fig. 2). **(a)** Time series of aerosol from inside-cabin PCASP and CDNC at 1 Hz and with 400 s binomial smoothing (red lines). Color bar indicates time in seconds. **(b)** Scatter plot of 1 Hz CDNC vs. PCASP N_{int}. Red line is least squares fit. **(c)** Scatter plot of high frequency anomaly (1 Hz signal – low frequency component) for CDNC vs. PCASP N_{int}. Red line is least squares fit. **(d)** Scatter plot of CDNC vs. PCASP after 10 s box car averaging. Points are color coded according to scale in "a" and are joined to indicate continuity. Note that the points fit within the envelope of points in panel "b" but appear more spread out because of a change of scale. **(e)** Scatter plot of CDNC vs. PCASP after 400 s binomial smoothing. Points are color coded as in "a" and "d".

ACPD
11, 17289–17336, 2011

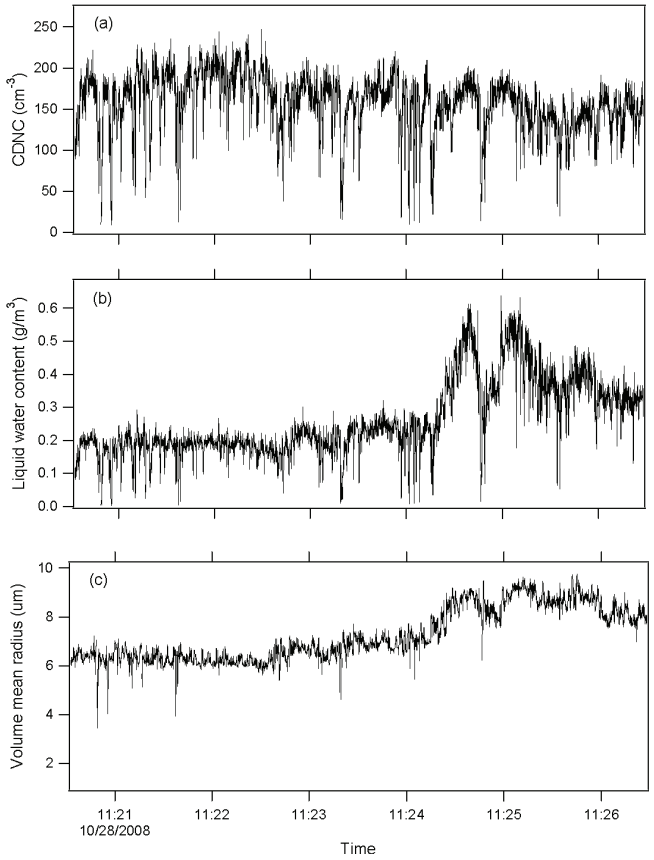

Fig. 14. (a) Cloud droplet number concentration, **(b)** liquid water content, and **(c)** cloud droplet volume mean radius for the same cloud transect and time period used in Fig. 13. Data collected at 10 Hz shows increased structure, in particular containing holes with near zero cloud droplet concentration and LWC. Distance covered is 35 km, comparable to the size of mesoscale structures apparent on satellite photos. Note change in cloud properties near 11:24:30.

ACPD
11, 17289–17336, 2011